Bioactive Materials 40 (2024) 430–444

Contents lists available at ScienceDirect

Bioactive Materials

journal homepage: www.keaipublishing.com/en/journals/bioactive-materials

Kneadable dough-type hydrogel transforming from dynamic to rigid network to repair irregular bone defects

Ningtao Wang [a,1], Jie Chen [b,1], Yanyang Chen [b], Liang Chen [b], Luhan Bao [b], Zhengmei Huang [c], Xiaoyu Han [b], Jiangkuo Lu [b], Zhengwei Cai [b,**], Wenguo Cui [b,*], Zhengwei Huang [a,***]

[a] Department of Endodontics, Shanghai Ninth People's Hospital, Shanghai Jiao Tong University School of Medicine, College of Stomatology, Shanghai Jiao Tong University, National Center for Stomatology, National Clinical Research Center for Oral Diseases, Shanghai Key Laboratory of Stomatology, 639 Zhizaoju Road, Shanghai, 200011, PR China

[b] Department of Orthopaedics, Shanghai Key Laboratory for Prevention and Treatment of Bone and Joint Diseases, Shanghai Institute of Traumatology and Orthopaedics, Ruijin Hospital, Shanghai Jiao Tong University School of Medicine, 197 Ruijin 2nd Road, Shanghai, 200025, PR China

[c] Department of Stomatology, Renji Hospital, Shanghai Jiao Tong University School of Medicine, 160 Pujian Road, Shanghai, 200127, PR China

ARTICLE INFO

Keywords:
Kneadable
Dough-type hydrogel
Dynamic network
Rigid network
Irregular bone defect

ABSTRACT

Irregular bone defects, characterized by unpredictable size, shape, and depth, pose a major challenge to clinical treatment. Although various bone grafts are available, none can fully meet the repair needs of the defective area. Here, this study fabricates a dough-type hydrogel (DR-Net), in which the first dynamic network is generated by coordination between thiol groups and silver ions, thereby possessing kneadability to adapt to various irregular bone defects. The second rigid covalent network is formed through photocrosslinking, maintaining the osteogenic space under external forces and achieving a better match with the bone regeneration process. *In vitro*, an irregular alveolar bone defect is established in the fresh porcine mandible, and the dough-type hydrogel exhibits outstanding shape adaptability, perfectly matching the morphology of the bone defect. After photocuring, the storage modulus of the hydrogel increases 8.6 times, from 3.7 kPa (before irradiation) to 32 kPa (after irradiation). Furthermore, this hydrogel enables effective loading of P24 peptide, which potently accelerates bone repair in Sprague–Dawley (SD) rats with critical calvarial defects. Overall, the dough-type hydrogel with kneadability, space-maintaining capability, and osteogenic activity exhibits exceptional potential for clinical translation in treating irregular bone defects.

1. Introduction

Bone defects caused by trauma, infection, tumor resection, and congenital diseases severely impact human health, causing heavy burdens on both society and families [1,2]. Irregular bone defects usually appear with random shapes, sizes, and depths. The irregular craniofacial bone defects would seriously affect the functions and aesthetics of patients, which is a critical challenge in stomatology [3,4]. Specifically, it is difficult to choose suitable materials that can fit the defective area's morphology and the surrounding tissues' physiological properties. Currently, autogenous bone blocks and xenogeneic granules are two predominant materials in stomatology. Autogenous bone blocks have excellent mechanical properties, resulting in outstanding space-maintaining capacity. However, the poor plasticity hinders them from implanting into irregular bone defects. Meanwhile, the limited resources and potential complications could also threaten their clinical application [5]. Xenogeneic granules can be used to fill the irregular bone defects by stacking these particles together, but their stability is unsatisfactory due to unsustainable integrity. External forces from flap closure, pressure of surrounding soft tissue, and movement of adjacent muscles can cause significant displacement of these granules, which leads to collapse of the osteogenic space and seriously affects the

Peer review under responsibility of KeAi Communications Co., Ltd.

* Corresponding author.
** Corresponding author.
*** Corresponding author.
E-mail addresses: caizhengwei@shsmu.edu.cn (Z. Cai), wgcui@sjtu.edu.cn (W. Cui), huangzhengwei@shsmu.edu.cn (Z. Huang).

[1] These authors contributed equally to this work.

https://doi.org/10.1016/j.bioactmat.2024.06.021
Received 24 February 2024; Received in revised form 23 May 2024; Accepted 11 June 2024

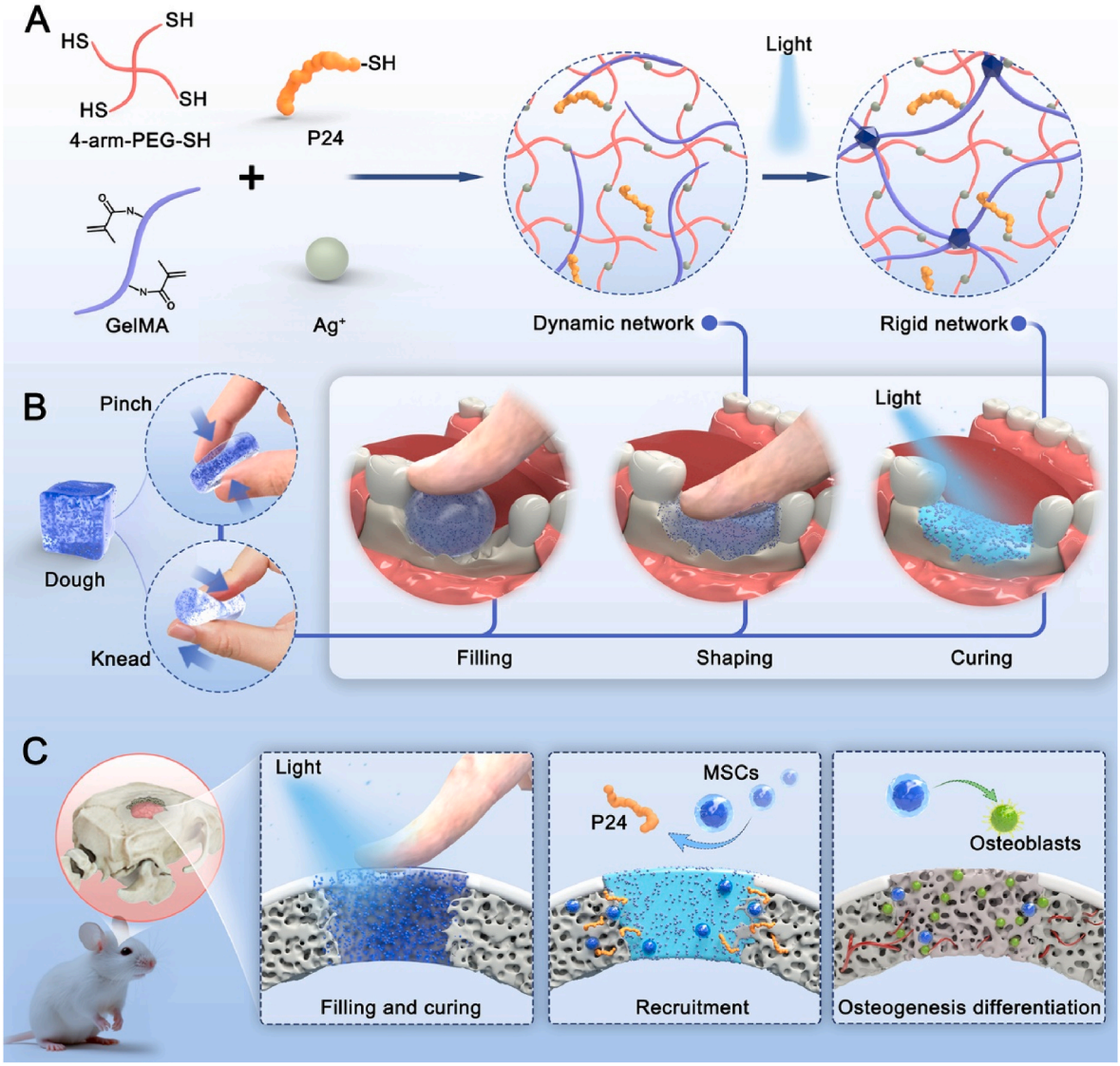

Scheme 1. Schematic diagram of the dough-type hydrogel for irregular bone defects repair. A) Synthesis process of the P24@DR-Net hydrogel. B) Dough-type properties of the P24@DR-Net hydrogel match the irregular bone defects. C) The enhanced osteogenesis in the rats with calvarial critical-size defect under the treatment of the P24@DR-Net hydrogel.

quantity of bone formation [6,7]. The contradiction between plasticity and the space-maintaining capability of these materials has always troubled clinicians [8]. Therefore, developing a bone-regenerative material possessing both of these properties is urgently necessary to treat irregular bone defects.

The behavior of bone cement materials is similar to that of construction cement [9]. The bone cement can be applied in bone defect areas with strong mechanical properties after the self-curing process [10]. As the most prevalent bone cements, polymethyl methacrylate (PMMA) bone cement and calcium phosphate cement (CPC) have widely attracted the attention of researchers [11,12]. Generally, PMMA bone cement has some advantages, including injectability and ease of use, but it also exhibits apparent drawbacks. For example, the curing process of PMMA bone cement would generate excessive heat and toxic polymer monomers. The PMMA bone cement also presents limited bioactivity, excessively high mechanical properties, and non-degradability [13,14]. Due to the similar inorganic compositions of bones, CPCs show excellent biocompatibility and osteoconductive properties, which have been comprehensively investigated [15,16]. However, CPCs suffer from poor mechanical properties, collapse in humid environments and short curing duration, which limits their clinical use [17–19]. Therefore, an ideal material is supposed to have the following characteristics: (1) satisfactory plasticity to adapt to irregular bone defects; (2) excellent biocompatibility and degradability; and (3) sufficient mechanical strength to maintain the space for bone formation and provide a sustained microenvironment for promoting osteogenic differentiation.

Recently, hydrogels have been widely investigated due to their controllable degradation rate, good manipulability, and adjustable mechanical properties [20–22]. Hydrogels are typically formed through various crosslinking methods to transit from solution to gelation, which can be applied in designing injectable biomaterials [23]. The injectable hydrogel has unique advantages when applied in the relatively closed anatomical space, as the precursor solutions can rapidly fill the targeted area. Then, the hydrogel can tightly integrate with the surrounding tissues after crosslinking [24–26]. However, many defective areas are uncontained bone defects, which lack bone walls [6]. The high fluidity of precursor solutions often leads to leakage in these defects. Moreover, most injectable hydrogels suffer from poor mechanical properties, which cannot maintain the spatial structure under external forces [27,28]. Therefore, it is meaningful to fabricate hydrogels that can match

irregular bone defects together with robust mechanical properties.

Inspired by the kneadability of dough, a sequentially crosslinked dough-type hydrogel (DR-Net) was designed in this study. The first dynamic hydrogel network was formed by the S–Ag coordinated bonds between thiol groups (4-arm-PEG-SH) and Ag ions, which makes the hydrogel kneadable to fill irregular bone defects in the mandibular alveolar bone. Subsequently, a rigid network was constructed *via in situ* photocuring of GelMA to enhance the mechanical properties, resist the external forces from the surrounding tissues, and maintain the space for osseous regeneration. Moreover, the synthetic peptide P24 derived from bone morphogenetic protein 2 (BMP-2) shows osteoinductivity similar to BMP-2, and has a thiol group at the cysteine residue that can dynamically bind to Ag^{+} in the DR-Net hydrogel [29]. Therefore, DR-Net hydrogel can effectively load P24 peptide, which exhibits excellent biocompatibility, degradability, and capability in enhancing the *in vitro* proliferation and osteogenic differentiation of MC3T3-E1 cells. Furthermore, accelerated new bone formation was observed in SD rats with critical calvarial defects treated with the dough-type hydrogel *in vivo* (Scheme 1). Overall, this study provides an innovative treatment approach for irregular bone defects in the future.

2. Materials and methods

2.1. Synthesis of the hydrogels

Dynamic-Network (D-Net): 0.1 g of 4-arm-PEG-SH (SINOPEG, Shenzhen, China) was dissolved in 0.5 mL of deionized water to prepare the 20 % (w/v) solution A at 37 °C. Subsequently, solution B, consisting of 0.5 mL of $AgNO_3$ (0.05 M, Aladdin, Shanghai, China), was added to solution A and thoroughly mixed to obtain the D-Net hydrogel.

Rigid-Network (R-Net): 0.1 g GelMA (Yongqinquan, Suzhou, China) was dissolved in 1 mL deionized water with photoinitiator LAP (0.25 %, w/v, Yongqinquan, Suzhou, China) to prepare the 10 % (w/v) GelMA solution at 37 °C. Then, the prepared GelMA solution was exposed to light for 60 s to obtain the R-Net hydrogel.

DR-Net: To prepare solution C, 0.1 g of 4-arm-PEG-SH (SINOPEG, Shenzhen, China) and 0.1 g of GelMA (Yongqinquan, Suzhou, China) were dissolved in 0.5 mL of deionized water containing the 0.5 % (w/v) photoinitiator LAP at 37 °C. Then, 0.5 mL solution B (0.05 M $AgNO_3$ solution), was mixed with solution C to obtain a first-crosslinked hydrogel as pre-DR-Net, which was further subjected to a second crosslinking process under light exposure for 60 s to form DR-Net.

P24@DR-Net: Peptide 24 (P24) (N→C: KIPKASSVPTELSAISTLYLSGGC) was synthesized by Apeptide Co., Ltd (Shanghai, China). Solution D was prepared by dissolving 0.1 g 4-arm-PEG-SH, 0.1 g GelMA, and 10 mg P24 peptide into 0.5 mL deionized water containing 0.5 % LAP at 37 °C. Subsequently, 0.5 mL solution B (0.05 M $AgNO_3$ solution), was mixed with solution D to obtain a first-crosslinked hydrogel. Finally, a second crosslinking process was achieved through 60 s light exposure, forming the P24@DR-Net hydrogel.

2.2. Characterization of the hydrogels

The D-Net, R-Net and DR-Net hydrogels were fixed on the copper table, then a thin layer of gold was sprayed. The scanning electron microscopy (SEM) (GeminiSEM 300, Zeiss, Germany) was utilized for observing the surface morphological characteristics of the hydrogels. The silver, sulfur, oxygen, carbon and nitrogen elements in DR-Net were then identified using energy dispersive X-ray spectroscopy (EDS) (GeminiSEM 300, Zeiss, Germany). Fourier-transform infrared spectroscopy (FTIR) (Nicolet iS20, Thermo Scientific, USA) was employed to analyze the different functional groups of each hydrogel sample within the wave number range of 400–4000 cm^{-1}. The X-ray Photoelectron Spectrometer (XPS) System (K-Alpha, Thermo Scientific, USA) was used to analyze the elemental compositions of the hydrogels.

2.3. Rheological measurements

First, stress-strain oscillations were conducted on the hydrogel to identify the critical strain required to disrupt the network of the hydrogel and transition it to a solution state at 37 °C and 60 % RH. And commercial fibrin glue (FG) was obtained from Shanghai RAAS Blood Products Co., LTD. (Shanghai, China) as a control. To observe the self-healing properties, changes in the storage modulus, loss modulus, and viscosity of the hydrogel were measured by a continuous step change of the strain 600 % and 0.5 % with a frequency of 10 rad/s at 37 °C and 60 % RH. The shear-thinning properties were tested at a shear rate of 0–320/s with a plate spacing of 0.3 mm at 37 °C and 60 % RH. The rheological curve of the photosensitive hydrogel was detected in situ by placing a 400 μL sample on the platform and subjecting it to irradiation (405 nm, 50 mW/cm^2) using the LED light source of the rotary rheometer at 37 °C and 60 % RH for 120 s.

2.4. Swelling and degradation testing of the hydrogel

The swelling test was calcuated as the following description. Hydrogels were immersed in deionized water and placed in a thermostatic shaker at 37 °C and 120 rpm. Then, the hydrogel was periodically weighed after the excess surface liquid was absorbed by the filter paper. The mass of the hydrogel at each time point was denoted as M_s, while the initial mass was recorded as M_0. The following formula calculated the swelling ratio: Swelling ratio $= M_s/M_0 \times 100$ %. For the degradation experiment in deionized water *in vitro*, the hydrogel mass after 24 h of swelling was denoted as M_a. The hydrogel was then incubated in deionized water in a thermostatic shaker at 37 °C and 120 rpm, and the mass at different time points was recorded as M_b. The degradation rate *in vitro* was calculated using the formula: Degradation Rate $= M_b/M_a \times 100$ %. For the degradation experiment in collagenase II solution, the R-Net and DR-Net hydrogels swelled for 24 h and were placed in the PBS solution containing 1 U/mL collagenase II in a thermostatic shaker at 37 °C and 120 rpm. The degradation rate of R-Net and DR-Net in the collagenase II solution was calculated using the above mentioned formula.

2.5. Release of P24@DR-Net hydrogel in vitro

To evaluate the release of P24 from the P24@DR-Net hydrogel, 200 μL of the P24@DR-Net hydrogel was initially immersed in 1 mL of PBS, after which the mixture was placed in a thermostatic shaker at 37 °C with a shaking speed of 120 r/min. At different intervals, the release solution (0.1 mL) was collected, and an equivalent volume of PBS solution was added. Concentration of P24 was detected using a BCA assay kit (Beyotime, China).

2.6. Cell culture

Mouse preosteoblasts (MC3T3-E1) were cultured at 37 °C and 5 % CO_2 atmosphere with alpha minimum essential culture medium (α-MEM) (GIBCO, USA) supplemented with 10 % fetal bovine serum (FBS) (GIBCO, USA) and 1 % penicillin-streptomycin (PS) (GIBCO, USA). The α-MEM culture medium was refreshed every 3 days. When the number of cells grew to 70–80 %, they were passaged for subsequent *in vitro* experiments. The cell experiments were performed with five groups: Control, D-Net, R-Net, DR-Net, and P24@DR-Net. Except the control group, the other groups were cultured in different hydrogel extracts.

2.7. Biocompatibility

To verify P24@DR-Net biocompatibility, we used live/dead cell staining, cytoskeleton staining, and CCK-8 proliferation assay for comprehensive evaluation of P24@DR-Net hydrogel effect on

proliferation and toxicity of mouse preosteoblasts (MC3T3-E1). 500 μL of hydrogel samples were immersed in 25 mL of α-MEM culture medium, and the hydrogel extracts of each group were collected at 24 h for MC3T3-E1 cell culture. First, the cell viability was detected on day 4 using the Cell Viability/Cytotoxicity Assay Kit (Beyotime, China), and the laser confocal microscope (Leica, Germany) was utilized to acquire the fluorescence image. Among them, dead cells are red, and living cells are green. Image J software counted the number of living and dead cells, and cell viability was defined as:

Cell Viability (%) = Living cell number / (Living cell number + Dead cell number).

In order to explore the influence of hydrogels on MC3T3-E1 cells adhesion and spreading. The study was carried out on the 5th day by skeleton staining. The cells were stained with F-actin tracker red-594 and 2-(4-aminophenyl)-6-indolecarbamidine dihydrochloride (DAPI) (Beyotime, China) to label F-actin and nucleus, respectively. A laser confocal microscope (Leica, Germany) was used to observe and take photos. To explore the proliferation of MC3T3-E1 cells, after 1, 4 and 7 days of incubation, the cell counting kit-8 (Beyotime, China) was utilized to assess the cell proliferation. The full wavelength microplate reader (Thermo Scientific, USA) was used to quantify the absorbance value (OD) at 450 nm.

2.8. Osteogenic differentiation in vitro

To assess the impact of the P24@DR-Net hydrogel on cell osteogenic

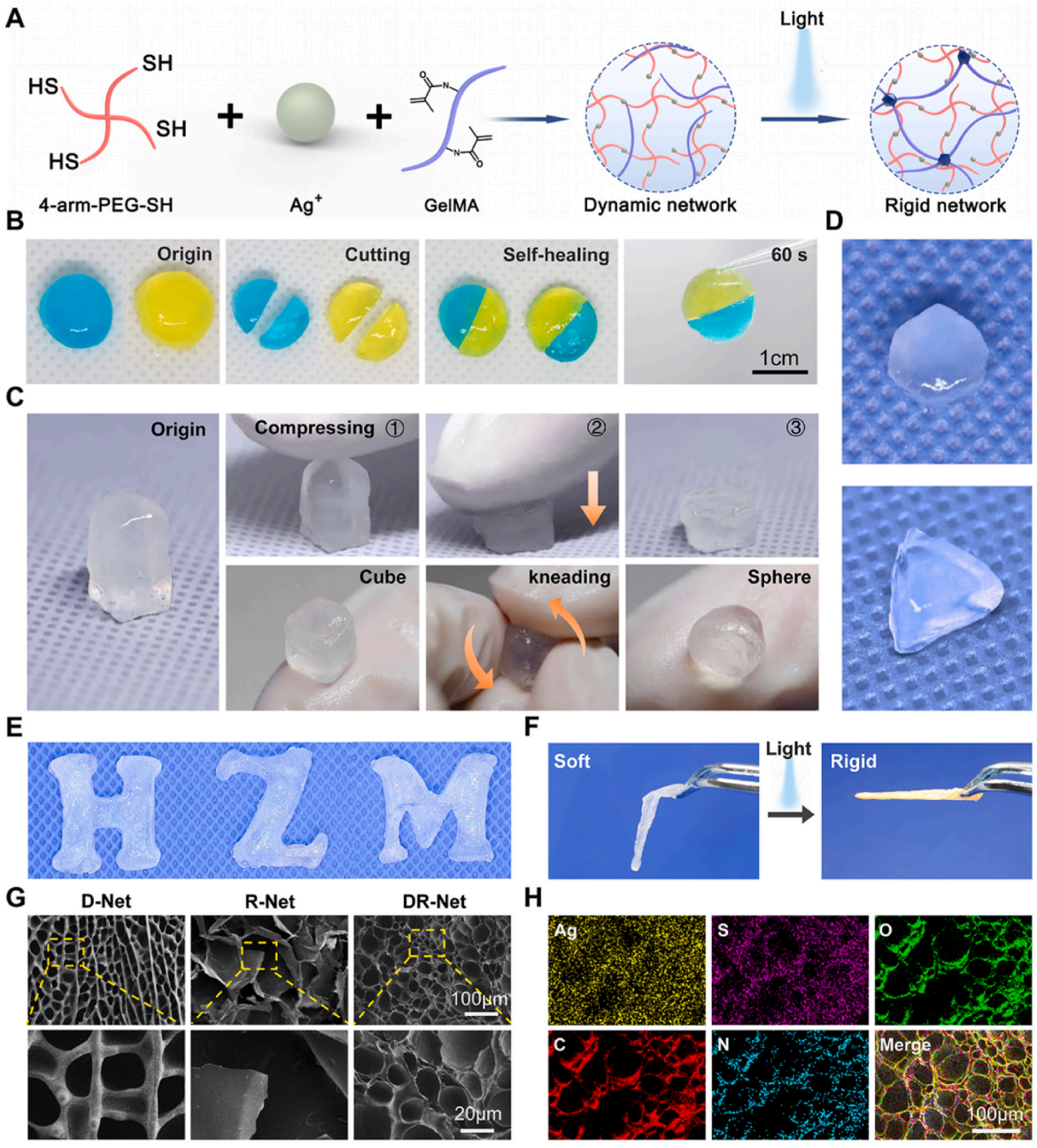

Fig. 1. Physicochemical properties of the DR-Net hydrogel. A) Schematic diagram of the synthesis of the DR-Net hydrogel. B) Illustration of self-healing properties of the pre-DR-Net hydrogel. C) Compressible and kneadable properties of pre-DR-Net. D, E) Photographs of pre-DR-Net molded into different shapes. F) Mechanical changes of the DR-Net hydrogel before and after irradiation. G) SEM morphology of the D-Net, R-Net and DR-Net hydrogels. H) EDS analysis of Ag, S, O, C and N elements in the DR-Net hydrogel.

differentiation, MC3T3-E1 cells were incubated with the hydrogel extracts in 24-well plates. After 7 days of *in vitro* culture, the MC3T3-E1 cells were treated with a 4 % paraformaldehyde solution. Subsequently, the samples were evaluated by alkaline phosphatase (ALP) staining kit (Beyotime, China) and observed by an inverted microscope. After 7 days of incubation, the cells were rinsed with PBS and then lysed to collect the supernatant by centrifugation. The ALP assay kit (Beyotime, China) was used to measure the ALP activity in each group.

To further assess the effect of the P24@DR-Net hydrogel on inducing mineralization, the cells were stained by an Alizarin Red S staining kit after 14 days of incubation, following fixation with 4 % paraformaldehyde. Then, the cells were photographed utilizing an inverted microscope. To quantify Alizarin Red S staining results, cells were incubated with 10 % cetylpyridine chloride (Solarbio, China) for 1 h, and the absorbance of suspension was quantified at 562 nm.

The osteogenic-related mRNA expression levels were detected utilizing RT-PCR to further validate the osteogenic differentiation effect of the P24@DR-Net hydrogel on MC3T3-E1 cells. After 7 days of culture, RNA was isolated from the cells by TRIzol reagent, followed by reverse transcription to obtain cDNA. The mRNA levels of Runx2, Col-1, ALP, OCN and OPN were detected and analyzed using a fluorescent quantitative PCR kit (Takara, Japan). The relative mRNA expression levels were normalized by the housekeeping gene glyceraldehyde-3-phosphate dehydrogenase (GAPDH) using the $^{\Delta\Delta}$Ct method, and the primer sequences are displayed in Table S1.

2.9. Animal models

In this study, all animal procedures were approved by the Animal Research Committee of Shanghai Jiao Tong University School of Medicine (SYXK 2018–0027). The research subjects were eight-week-old male SD rats weighing approximately 280 g. The rats were randomly divided into 5 groups (6 rats per group): the control group, D-Net group, R-Net group, DR-Net group, and P24@DR-Net group. Before surgery, the rats were administered anesthesia by intraperitoneally injecting pentobarbital sodium solution (50 mg/kg) and immobilized on the surgical table upon loss of reflex reactions. After that, the hair surrounding the surgical area was shaved to ensure complete skull exposure and disinfected using an iodine solution. 5 mm diameter bone defects were drilled with an electric drill at a relatively flat position on the skull. The hydrogels were subsequently implanted in situ and R-Net, DR-Net, and P24@DR-Net were crosslinked by light irradiation. Following completion of the crosslinking, the muscles and skin were sutured with a 5–0 thread. After 4 and 8 weeks of implantation, the rats were euthanized by carbon dioxide asphyxiation. The skull samples were subsequently collected and fixed in a 4 % paraformaldehyde solution for 24 h.

2.10. Micro-CT evaluation

Micro-CT was used to scan the rats' skulls collected at 4 and 8 weeks, and three-dimensional reconstruction and quantitative statistical analysis were performed. Bone defect healing was assessed based on the quantification of bone volume/tissue volume (BV/TV), trabecular number (Tb.N), trabecular thickness (Tb.Th), and trabecular separation (Tb.Sp).

2.11. Histological evaluation

To further evaluate *in vivo* bone formation, decalcification was performed on the collected rat skull samples at 4 and 8 weeks, followed by the preparation of paraffin tissue specimens. Subsequently, 5 μm thick sections obtained using a microtome were subjected to H&E, Masson, and immunofluorescence staining. Immunostaining was performed by permeabilizing skull sections in 0.1 % Triton X-100 for 15 min. Then, the skull sections were blocked with 5 % goat serum at room temperature for 30 min, followed by incubating with primary antibody overnight at 4 °C. Primary antibody: OCN (GB11233-100, Servicebio, China) and Col-1 (GB11022-3-100, Servicebio, China). Afterward, the sections were thoroughly washed with PBS and incubated with secondary antibodies at room temperature. Additionally, nuclear counterstaining was achieved using DAPI. Confocal microscope and ImageJ software were used to observe and quantify the fluorescence image, respectively.

2.12. Statistical analysis

The experimental data were presented as mean and standard deviation after at least three repetitions of each segment. Origin and GraphPad Prism 9.5.1 were utilized for statistical analysis. The experimental data among groups were compared utilizing One-way analysis of variance (ANOVA) with Tukey's post hoc analysis. A statistically significant difference was defined as P value < 0.05.

3. Results and discussion

3.1. The preparation and characterization of DR-net hydrogel

Hydrogels composed of a dynamic network *via* metal–ligand coordination exhibit high adaptability to the physical properties of natural tissues in tissue engineering [30,31]. On the other hand, photocrosslinking hydrogels can be synthesized by photochemical reactions, such as free radical polymerization and click chemistry, forming a rigid covalent network, which have excellent mechanical properties [32–34]. To fabricate a sequentially crosslinked hydrogel with both kneadability and space-maintaining capability, we performed the first dynamic network between the thiol groups of 4-arm-PEG-SH and silver ions due to their high affinity. This first crosslinked hydrogel, called pre-DR-Net, was a dough-type hydrogel with superb kneadability. Furthermore, the second rigid network was conducted through the photoinitiated free radical polymerization of gelatin methacrylate (GelMA) to form the DR-Net hydrogel with significantly enhanced mechanical properties (Fig. 1A).

To explore the self-healing capability of the first dynamic network of DR-Net (pre-DR-Net), two hydrogels with different colors (blue and yellow) were prepared (Fig. 1B). These two hydrogels were cut in half and placed together. After 60 s, these two hydrogels (blue and yellow) were fused into a whole without any apparent interface. Furthermore, when the hydrogel was lifted, the incision did not split, demonstrating that the interaction force was sufficient to bear the weight of the other half of the hydrogel. Further, we made a scratch on the pre-DR-Net hydrogel and captured the self-healing interface of the hydrogel under a stereo microscope. As illustrated in Fig. S1, the scratch on pre-DR-Net hydrogel autonomously healed within 50 s. The self-healing capability of pre-DR-Net could be attributed to the dynamic and reversible S–Ag coordination between thiol groups and silver ions [35].

In addition, the pre-DR-Net hydrogel showed similar properties to the dough (Movie S1), which can be kneaded and shaped to any morphology. As shown in Fig. 1C, the pre-DR-Net hydrogel could be compressed without a noticeable rebound. Subsequently, the hydrogel was kneaded from a cubic form into a spherical shape. Furthermore, the pre-DR-Net hydrogel could fill molds with various shapes, such as hexagons, triangles, and letters as shown in Fig. 1D and **E**. The intriguing properties of pre-DR-Net hydrogel make it a suitable candidate for treating irregular bone defects. Then, the mechanical characteristics of DR-Net hydrogel were evaluated before and after photoinitiated crosslinking. As shown in Fig. 1F, the pre-DR-Net hydrogel was soft and compliant with limited mechanical strength before irradiation. Under the influence of gravity, the pre-DR-Net hydrogel was noticeably curved. In contrast, the double-network DR-Net hydrogel exhibited no significant deformation owning to the new formation of the rigid covalent network, which indicates that the DR-Net hydrogel could effectively maintain the spatial structure after the implantation compared to the pre-DR-Net hydrogel.

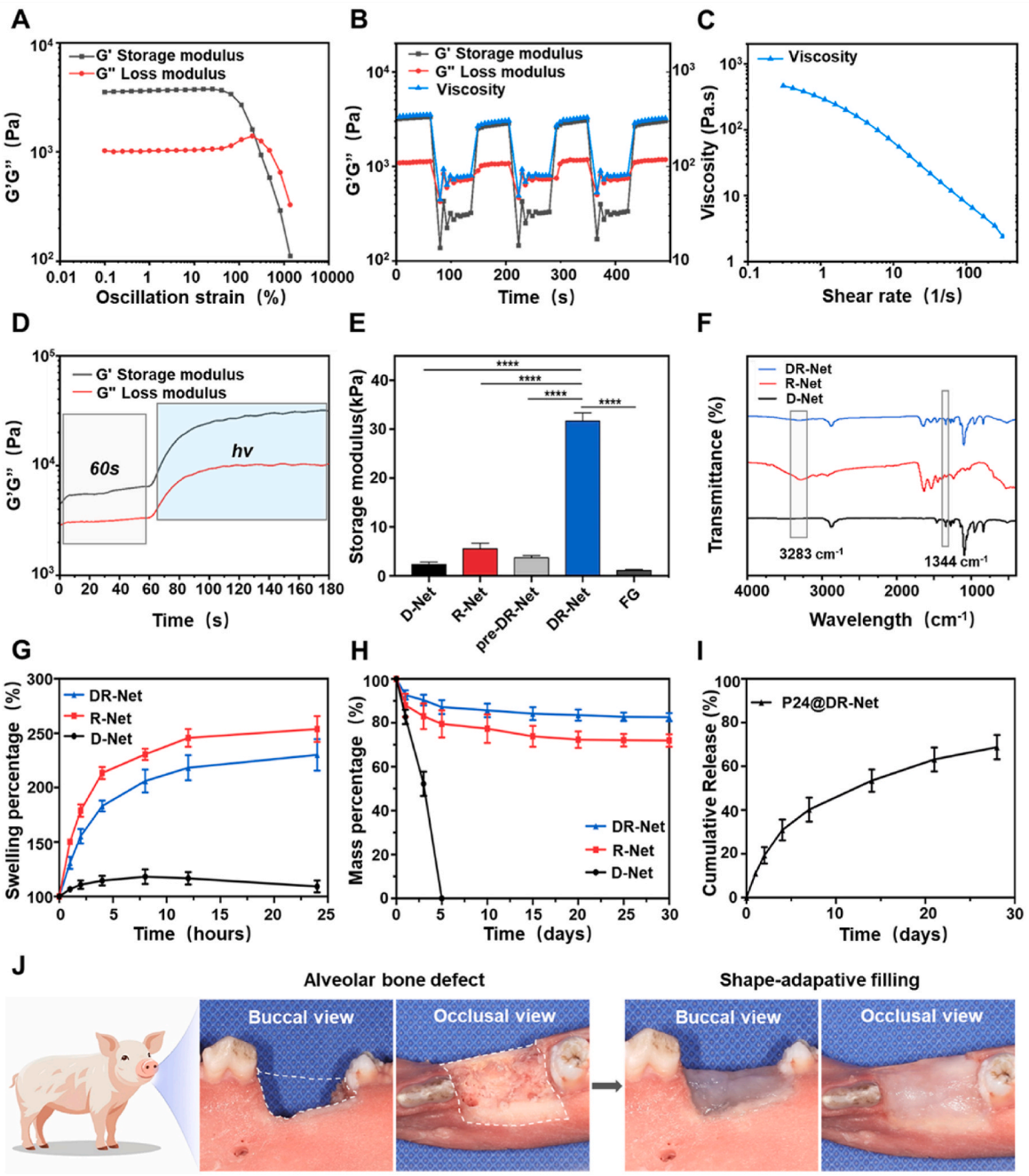

Fig. 2. Characterization of the hydrogels. A) Strain sweep measurements of G' (storage modulus) and G" (loss modulus) of pre-DR-Net. B) Dynamic step-strain measurements of pre-DR-Net *via* repeated deformation of 0.5 % strain for 60s and 600 % strain for 60s. C) The different viscosity of pre-DR-Net varies with shear rate. D) Change of G′ and G″ of DR-Net *via* irradiation for 120s. E) Comparison of storage modulus of D-Net, R-Net, pre-DR-Net, DR-Net and FG, n = 3. F) FTIR spectrum of D-Net, R-Net and DR-Net. G) Swelling curves and H) Degradation behavior of the hydrogels, n = 3. I) The release behavior of P24 peptide from the P24@DR-Net hydrogel, n = 3. J) The shape-adaptive filling of pre-P24@DR-Net hydrogel in the irregular defect of the fresh porcine mandibular alveolar bone.

Supplementary data related to this article can be found at https://doi.org/10.1016/j.bioactmat.2024.06.021.

Afterward, we synthesized the dynamic network hydrogel (D-Net) and the rigid network hydrogel (R-Net). D-Net was formed by the S–Ag coordination between 4-arm-PEG-SH and silver ions, and R-Net was synthesized by the photoinitiated radical polymerization of GelMA. The morphologies of DR-Net, D-Net, and R-Net hydrogels were explored by the scanning electron microscopy (SEM). These three hydrogels were porous with sponge-like structures and interconnected channels (Fig. 1G). The porous structure is similar to the natural extracellular matrix (ECM), which benefits the cell adhesion and proliferation [36,37]. Moreover, the DR-Net had a rougher and denser morphology than the D-Net and R-Net hydrogels (1000 × magnification), which would facilitate the adhesion of osteoblasts [38]. Additionally, according to the energy dispersive X-ray spectroscopy (EDS) analysis of the DR-Net hydrogel, Ag, S, O, C, and N elements homogenously distributed in the DR-Net hydrogel, confirming the successful formation of the hydrogel networks *via* dynamic coordinated crosslinking (between silver ions and 4-arm-PEG-SH) and photocrosslinking (GelMA) (Fig. 1H).

The rheological analysis further evaluated the mechanical properties of these hydrogels (D-Net, R-Net, and DR-Net). As shown in Fig. 2A, the first crosslinked pre-DR-Net hydrogel exhibited higher storage modulus

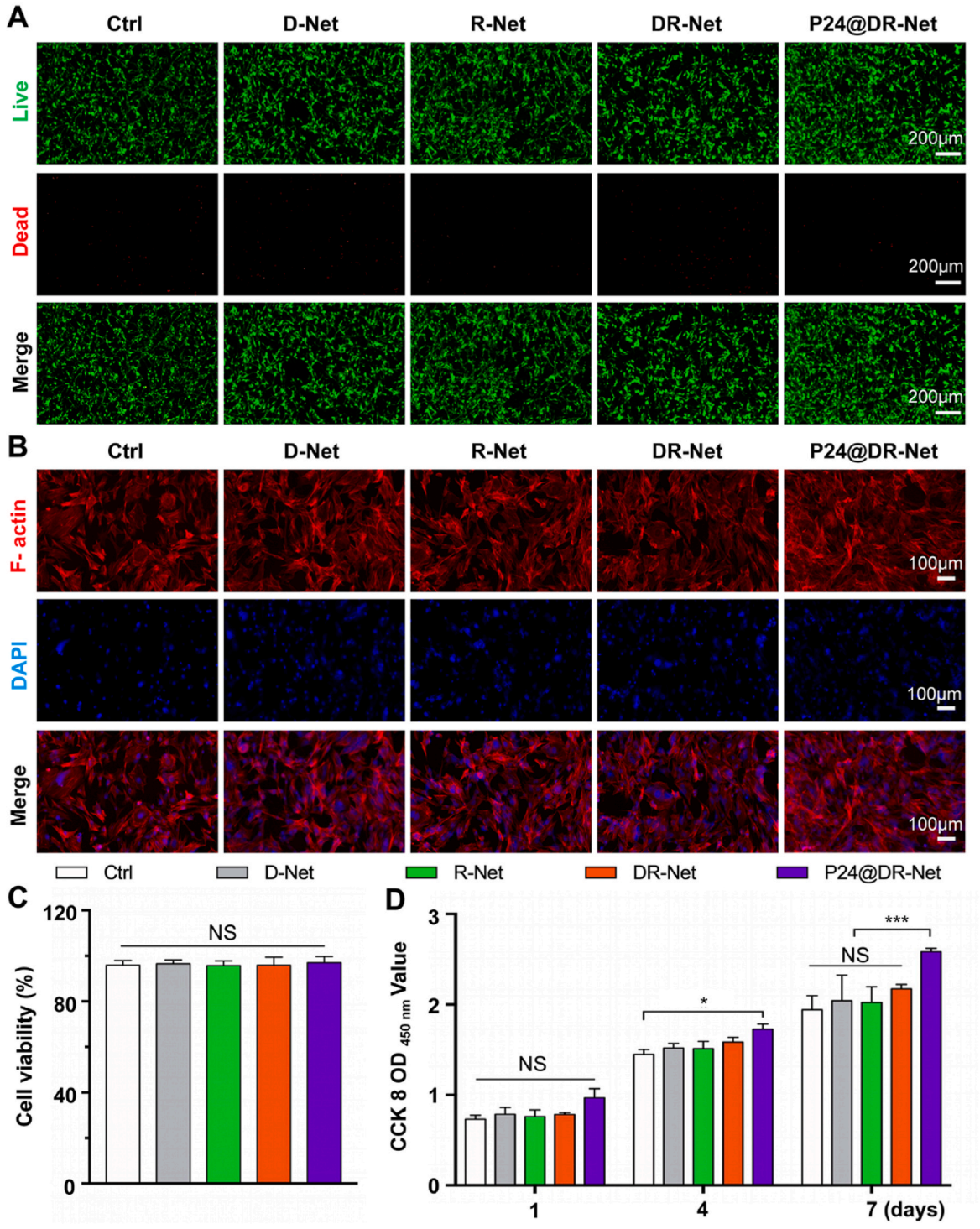

Fig. 3. The biocompatibility of the hydrogels *in vitro*. A) Representative live/dead staining images of MC3T3-E1 cells cultured with hydrogel extracts on day 4. B) Cytoskeleton morphology of MC3T3-E1 cells treated with hydrogel extracts for 5 days. C) Semi-quantitative analysis of cell viability, as assessed using the live/dead assay. D) The CCK-8 values. (*$p < 0.05$ and ***$p < 0.001$. "NS", no statistical significance. Data are presented as mean ± SD, n = 3. One-way ANOVA followed by Tukey's post hoc analysis was used).

and lower loss modulus, indicating the gel state. Then, the storage modulus gradually decreased with the increased shear strain. The hydrogel showed a flow state when the shear strain reached 227 %. Additionally, the self-healing properties of pre-DR-Net were assessed by the dynamic step-strain measurements. As depicted in Fig. 2B, the storage modulus (G′) exhibited a notable decline, decreasing from approximately 3000 Pa–300 Pa, and the viscosity decreased from 300 Pa s to 80 Pa s during the strain transition from 0.5 % to 600 %. When the strain was reduced from 600 % to 0.5 %, the viscosity and modulus of the hydrogel could recover within a few seconds. In addition, we further performed 20 cycles of dynamic step-strain measurements on the pre-DR-Net hydrogel, and the results showed that the pre-DR-Net hydrogel still maintained excellent resilience (Fig. S2). Moreover, the shear rate gradually increased with a decreased viscosity of pre-DR-Net,

indicating the shear-thinning property of this first crosslinked hydrogel (Fig. 2C). These findings revealed that the dynamic metal coordinated bonds between silver ions and thiol groups were weakened with enhanced external stress, resulting in a decrease in the storage modulus and viscosity of the hydrogel. Once the external stress was removed, the dynamic metal coordinated bonds were re-established with the restoring mechanical properties of the hydrogel. Similar phenomena were also observed in D-Net (Figs. S3 and S4).

Furthermore, the photocrosslinking behavior of DR-Net and R-Net was investigated under the irradiation. As shown in Fig. 2D, pre-DR-Net was processed with the first crosslinking. After 60 s of the first crosslinking, an LED light source (405 nm, 50 mW/cm^2) was used to conduct the second crosslinking to form DR-Net hydrogel for 120 s. The storage modulus (G′) of the DR-Net rapidly increased and reached equilibrium after approximately 60 s of light exposure. The R-Net precursor solution was directly crosslinked for 120 s with the storage modulus (G′) increased to (≈5.5 kPa) (Fig. S5). According to the rheological results, the storage modulus (G′) of DR-Net (G'≈ 32 kPa) was significantly higher than that of D-Net (G'≈ 2.4 kPa), R-Net (G'≈ 5.5 kPa), pre-DR-Net (G'≈ 3.7 kPa) and FG (G'≈1.1 kPa), which meant the modulus of DR-Net increased by 8.6 times after irradiation and was 29 times that of FG (Fig. 2E, **S6**). These results indicate that DR-Net hydrogel is a hybrid system consisting of dynamic and rigid networks with mechanical properties that are not simply the sum of D-Net and R-Net.

Further, the hydrogel structure was explored by Fourier transform infrared (FTIR) spectroscopy. The characteristic peak of the S–Ag coordination bonds was identified at 1344 cm^{-1} in D-Net and DR-Net hydrogels, which is the critical mechanism in forming the dynamic network. Meanwhile, the characteristic peak of –NH_2 (GelMA) was observed at 3283 cm^{-1} in both R-Net and DR-Net hydrogels, suggesting both the dynamic network of D-Net and the rigid network of R-Net appearing in the DR-Net hydrogel (Fig. 2F). Moreover, based on the X-ray photoelectron spectroscopy (XPS) findings, both the DR-Net and D-Net hydrogels contained the Ag element (Fig. S7). Meanwhile, DR-Net hydrogel had the same N element as R-Net. These results also reveal the coexistence of the D-Net and R-Net in the DR-Net hydrogel.

The swelling capacities of D-Net, R-Net, and DR-Net hydrogels were evaluated by calculating the swelling rate at different time points. After incubating for 24 h, the D-Net, R-Net, and DR-Net exhibited swelling rates of 109.56 ± 5.78 %, 253.87 ± 11.94 %, and 230.08 ± 15.53 %, respectively (Fig. 2G), which indicated these hydrogels could have excellent water retention ability. Notably, D-Net hydrogel reached a swelling balance after only 8 h of incubation. Afterward, the hydrogel network began to degrade. In the degradation experiments, the D-Net hydrogel totally degraded after 5 days of incubation in deionized water, which meant that the D-Net hydrogel could be unstable *in vivo* and unable to match the regeneration process of bone tissue. In contrast, R-Net and DR-Net hydrogels retained approximately 75 % and 85 % of the original mass even after 30 days of incubation in deionized water (Fig. 2H). Furthermore, since R-Net and DR-Net hydrogels contained GelMA, they were incubated in a phosphate-buffered saline (PBS) solution with collagenase II. The R-Net hydrogel completely degraded within 3 days, while DR-Net took 11 days (Fig. S8). The DR-Net group exhibited the slowest degradation rate *in vitro*, demonstrating that the double networks could effectively enhance the stability of the hydrogel, and of course the degradation rate was also correlated with the concentration of collagenase. As is well known, the bone healing is a slow and complex process, which can be divided into four different phases: hematoma phase, cartilaginous callus formation phase, bony callus formation phase and bone remodeling phase, and this process lasts for 8–16 weeks [39,40]. Therefore, compared with D-Net and R-Net, the degradation rate of DR-Net will better match the bone formation rate, which gradually decomposes with the formation of new tissues.

Currently, most bone-tissue engineering scaffolds lack osteoinductivity, so it is necessary to introduce growth factors [41]. The synthetic peptide P24 is derived from bone morphogenetic protein-2 (BMP-2), demonstrating osteoinductivity similar to BMP-2 [42]. Compared to the BMP-2, P24 exhibits higher specificity and fewer side effects [43]. Additionally, P24 has thiol groups at the cysteine residue that can dynamically bind with Ag^+ in DR-Net, guaranteeing the dynamic release of P24. Therefore, we incorporated P24 into the DR-Net hydrogel to prepare the osteoinductive hydrogel (P24@DR-Net). As shown in Fig. 2I, the P24 release behavior was evaluated in a phosphate-buffered saline (PBS) solution. During the first 7 days, 40 % of P24 peptide underwent a burst release. Subsequently, the release rate gradually decreased. After 28 days, about 70 % of the P24 peptide was released. The burst release could be attributed to the initial swelling of the P24@DR-Net hydrogel upon contact with the PBS solution, leading to an expansion of the hydrogel network and facilitating the rapid release of P24. Then, the stable double-crosslinked hydrogel networks guaranteed the constant release of P24 in the following days. Additionally, an irregular alveolar bone defect was established in the fresh porcine mandible (Fig. 2J). The pre-P24@DR-Net hydrogel exhibited outstanding shape adaptability after the first crosslinking, perfectly matching the morphology of the bone defect without collapse under the influence of gravity. Then, the hydrogel was processed with photocuring to enhance the mechanical performance. Afterward, the filling area was rinsed with fast-flowing water. As expected, P24@DR-Net could withstand the external force without displacement or collapse in situ, maintaining the spatial shape and structure for bone regeneration (Movie S2). In contrast, D-Net hydrogel quickly collapsed after filling irregular bone defects, while R-Net hydrogel precursor failed to fill uncontained bone defects and flowed out along the low edge of the bone wall. In addition, we further compared them with FG, although FG has injectable capability, it cannot effectively fill uncontained alveolar bone defects. In addition, the gelation rate of fibrin glue is too fast for kneading and shaping (Fig. S9). Therefore, P24@DR-Net demonstrates the optimal shape adaptability and space-maintaining capability.

Supplementary data related to this article can be found at https://doi.org/10.1016/j.bioactmat.2024.06.021.

3.2. Biocompatibility assessment of the P24@DR-Net hydrogel in vitro

The P24@DR-Net hydrogel, as a promising kneadable bone-promoting biomaterial, requires good biocompatibility. Therefore, mouse preosteoblasts (MC3T3-E1) were cultured in different hydrogel extraction solutions for three experiments to evaluate the biocompatibility of the hydrogels. After 4 days of incubation, we performed live/dead staining on the cells. As shown in Fig. 3A, a few dead cells were indicated by red fluorescence in each group. In contrast, most MC3T3-E1 cells exhibited viability indicated by green fluorescence, with good cellular morphology and vitality. According to a statistical analysis on the populations of live and dead cells, the cell viability consistently remained above 95 % in all the experimental groups, with no statistically significant differences (Fig. 3C). On the 5th day, the spreading and morphology of cells were observed by skeleton/nucleus fluorescence staining. The cytoskeleton was clear in all groups, without significant differences in the spread area of the cells (Fig. 3B). Then, the cell proliferation was quantified by the cell counting kit-8 on day 1, 4 and 7. As shown in Fig. 3D, no dramatic difference was observed in the absorbance value (450 nm) of each group after 1 day of culture. However, on days 4 and 7, the findings demonstrated that the P24@DR-Net hydrogel effectively enhanced the proliferation of the cells. To sum up, the P24@DR-Net hydrogel exhibits good biocompatibility and can promote cell proliferation.

3.3. Osteogenic properties evaluation of the P24@DR-Net hydrogel in vitro

To investigate the impact of the P24@DR-Net hydrogel on osteogenic differentiation of MC3T3-E1 cells, the cells were incubated with extraction solutions from various hydrogel groups. Subsequently,

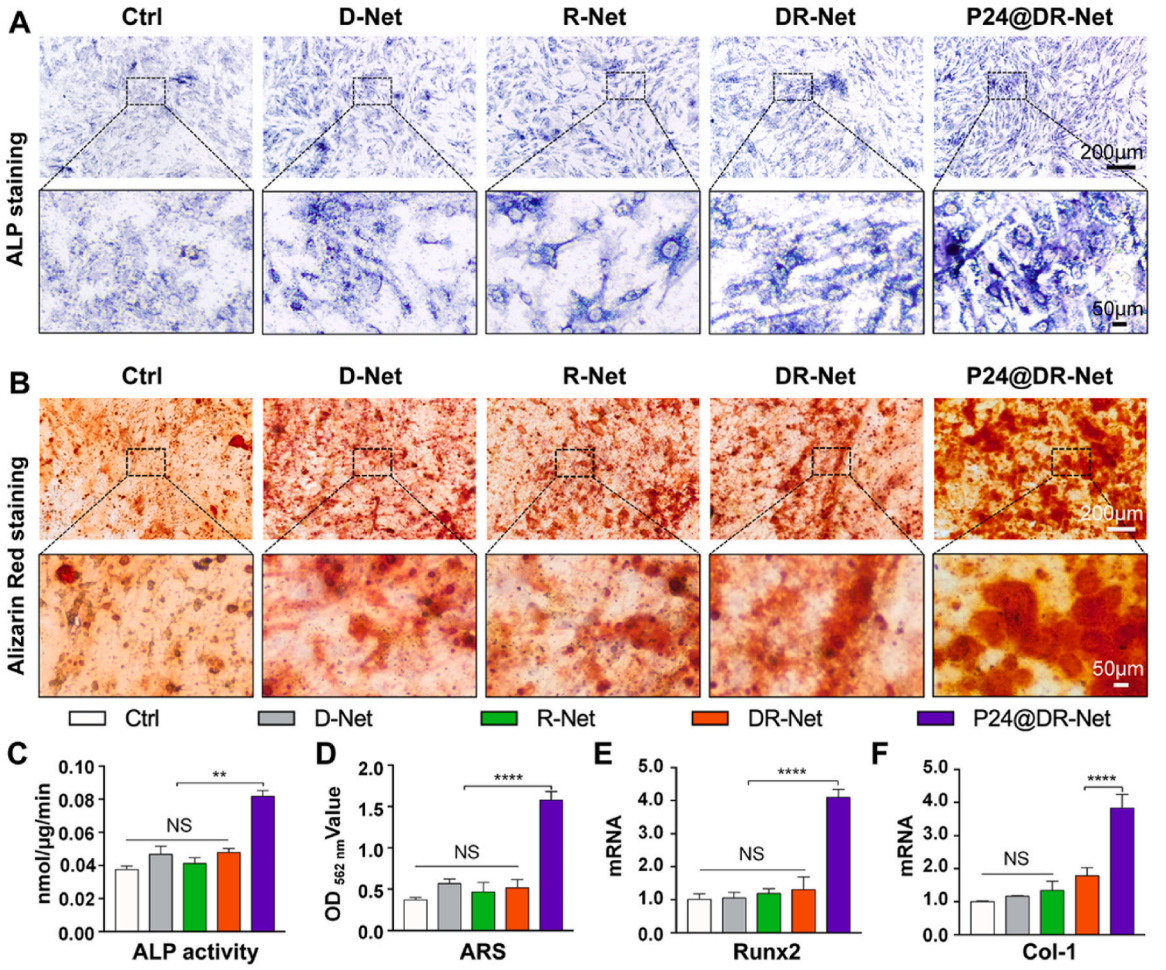

Fig. 4. The osteogenic effect of the hydrogels *in vitro*. A) The ALP staining images of MC3T3-E1 cells cultured with different hydrogel extracts for 7 days. B) The Alizarin Red S staining images of MC3T3-E1 cells cultured with different hydrogel extracts for 14 days. C) Semi-quantitative analysis of ALP activity. D) Quantified results of calcified nodules. The mRNA relative expression levels of E) Runx2 and F) Col-1 gene in MC3T3-E1 cells treated with different hydrogel extracts for 7 days. (**$p < 0.01$ and ****$p < 0.0001$. "NS", no statistical significance. Data are presented as mean ± SD, n = 3. One-way ANOVA followed by Tukey's post hoc analysis was used).

osteogenic differentiation performance was further detected using alkaline phosphatase (ALP) staining and Alizarin Red S (ARS) staining [44–46]. ALP, a widely recognized early osteogenic differentiation marker, is a crucial enzyme in osteogenic differentiation [47,48]. ALP can react with organic phosphates, raising the local concentration of PO_4^{3-} [49]. Additionally, it can bind to Ca^{2+} to regulate the mineralization of the bone matrix [50]. As shown in Fig. 4A, after 7 days of incubation, the P24@DR-Net group exhibited more intense ALP staining than the control group and the other hydrogel groups. This showed that P24@DR-Net hydrogel could promote osteogenic differentiation of MC3T3-E1 cells. Furthermore, the P24@DR-Net hydrogel had higher ALP activity than the other groups, according to the ALP activity assays (Fig. 4C). In summary, these findings suggest that the release of P24 facilitated osteogenic differentiation of MC3T3-E1 cells. A similar trend was observed for ARS staining. The control, D-Net, R-Net, and DR-Net groups exhibited irregularly shaped and small-volume red calcified nodules that were loosely scattered, after 14 days of osteogenic culture. Conversely, a large number of clustered red calcified nodules were observed in the P24@DR-Net group (Fig. 4B). These findings suggested that the release of P24 promoted the osteogenic activity of MC3T3-E1 and enhanced bone matrix mineralization. As shown in Fig. 4D, the P24@DR-Net group exhibited significantly higher values compared to the other groups, according to the quantified results of ARS staining. The result was consistent with the observed staining outcomes.

The complex process of osteogenic differentiation involves multiple interrelated regulatory variables. Runt-related transcription factor 2 (Runx2), a crucial gene involved in osteogenesis, is responsible for regulating the formation of bone tissue [51,52]. Type 1 collagen (Col-1), an essential component of the bone ECM, plays a vital role in facilitating the interaction between cell surface receptors and ECM proteins [53]. Consequently, we assessed the expression levels of osteogenic genes (Runx2, Col-1, ALP, OCN and OPN) to further evaluate the hydrogels. The P24@DR-Net group exhibited significantly higher mRNA levels of osteogenesis genes than other groups, according to Fig. 4E, **F** and **S10**. These results further validated the effectiveness of the P24@DR-Net hydrogel in enhancing the osteogenic differentiation of MC3T3-E1 cells.

3.4. Osteogenic effects of P24@DR-Net hydrogel in vivo

To evaluate the efficacy of the P24@DR-Net hydrogel in repairing bone defects *in vivo*, an SD rat model with critical-sized calvarial defects measuring 5 mm was established for *in vivo* osteogenesis experiments (Fig. 5A–C) [54,55]. The groups were divided into control, D-Net, R-Net, DR-Net, and P24@DR-Net *in vivo*. Among them, DR-Net and P24@DR-Net were crosslinked twice, improving the hydrogel networks' strength and providing better mechanical support for subsequent bone

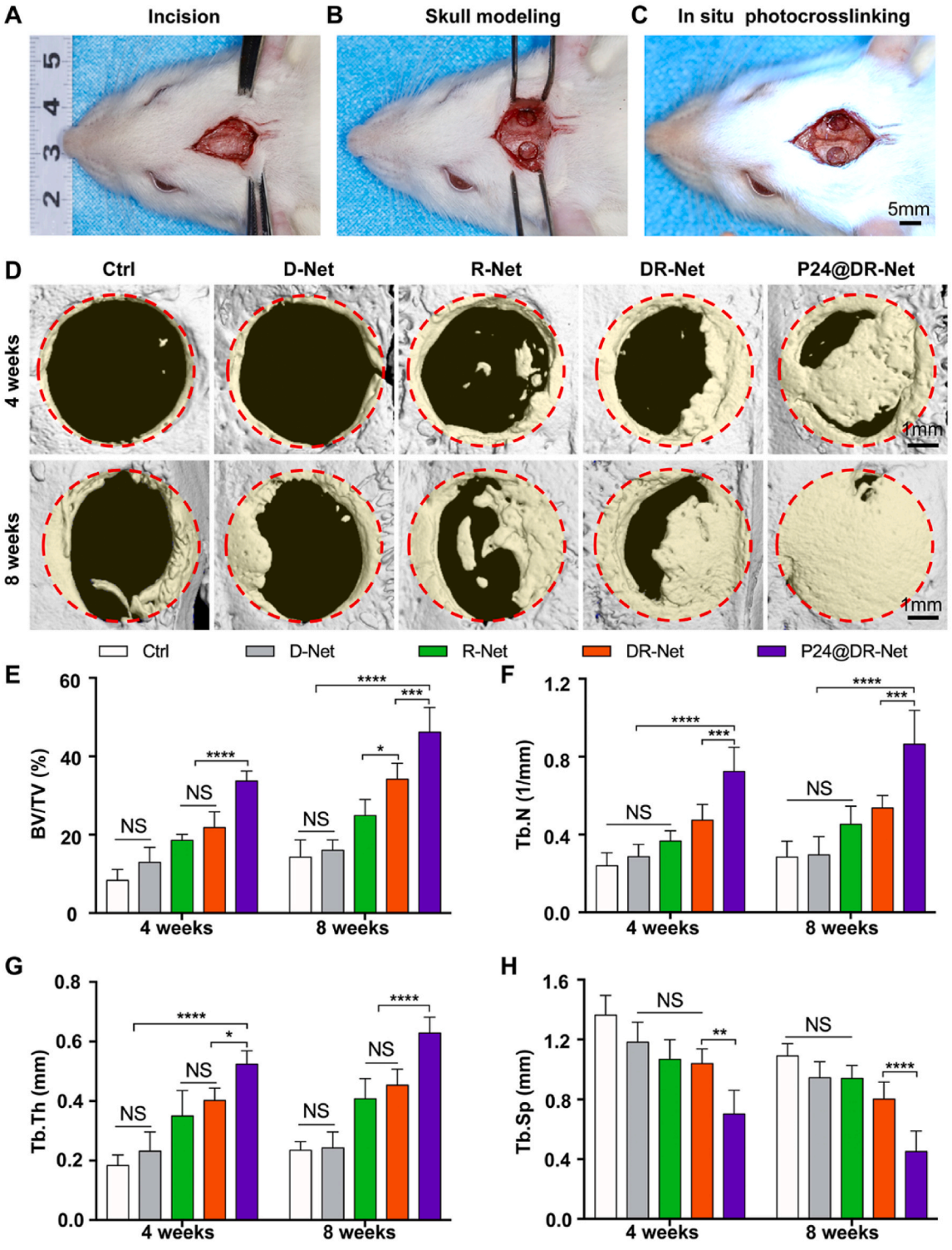

Fig. 5. The osteogenic effect of the hydrogels *in vivo*. A-C) The establishment of the calvarial defect model (size, 5 mm) in SD rats and the implantation of hydrogels. D) The 3D Micro-CT reconstructions of defect area at 4 and 8 weeks after implantation. E-H) BV/TV, Tb.N, Tb.Th and Tb. Sp determined by Micro-CT. (*$p < 0.05$, **$p < 0.01$, ***$p < 0.001$ and ****$p < 0.0001$. "NS", no statistical significance. Data are presented as mean ± SD, n = 6. One-way ANOVA followed by Tukey's post hoc analysis was used).

formation. At 4 and 8 weeks after surgery, the rat calvarial defect areas were scanned and analyzed by Micro-CT. Micro-CT reconstruction techniques were employed for the three-dimensional reconstruction of bone defects to observe the defect area precisely and further quantify the new bone mass. Bone morphometry was then utilized to analyze BV/TV, Tb.Th, Tb.N, and Tb. Sp across all groups [56,57]. As illustrated in Fig. 5D, new bone formation appeared from the defect edge to the center in all hydrogel groups, with a gradually reduced calvarial defect area. At 4 and 8 weeks, the control group and D-Net group exhibited limited new bone generation only at the periphery of the bone defect, whereas other

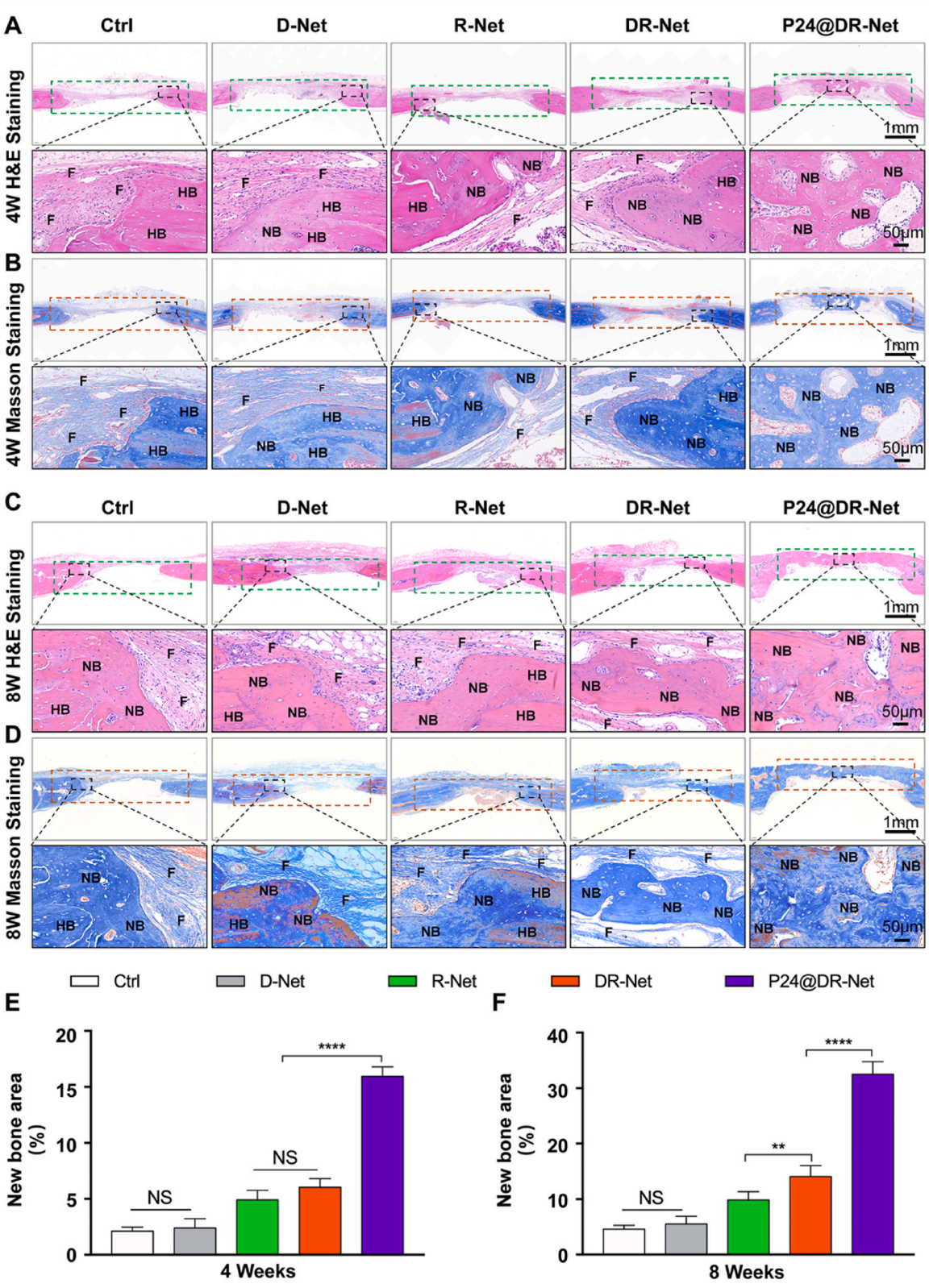

Fig. 6. Histological evaluation of the hydrogels *in vivo*. A, C) Representative H&E-stained images at 4 and 8 weeks after operation. B, D) Representative Masson-stained images at 4 and 8 weeks. E, F) Semi-quantitative analysis of new bone area in each group. (new bone: NB, fibrous tissue: F, and host bone: HB, with the area of the bone defect within the dashed box. $^{**}p < 0.01$ and $^{****}p < 0.0001$. "NS", no statistical significance. Data are presented as mean ± SD, n = 6. One-way ANOVA followed by Tukey's post hoc analysis was used).

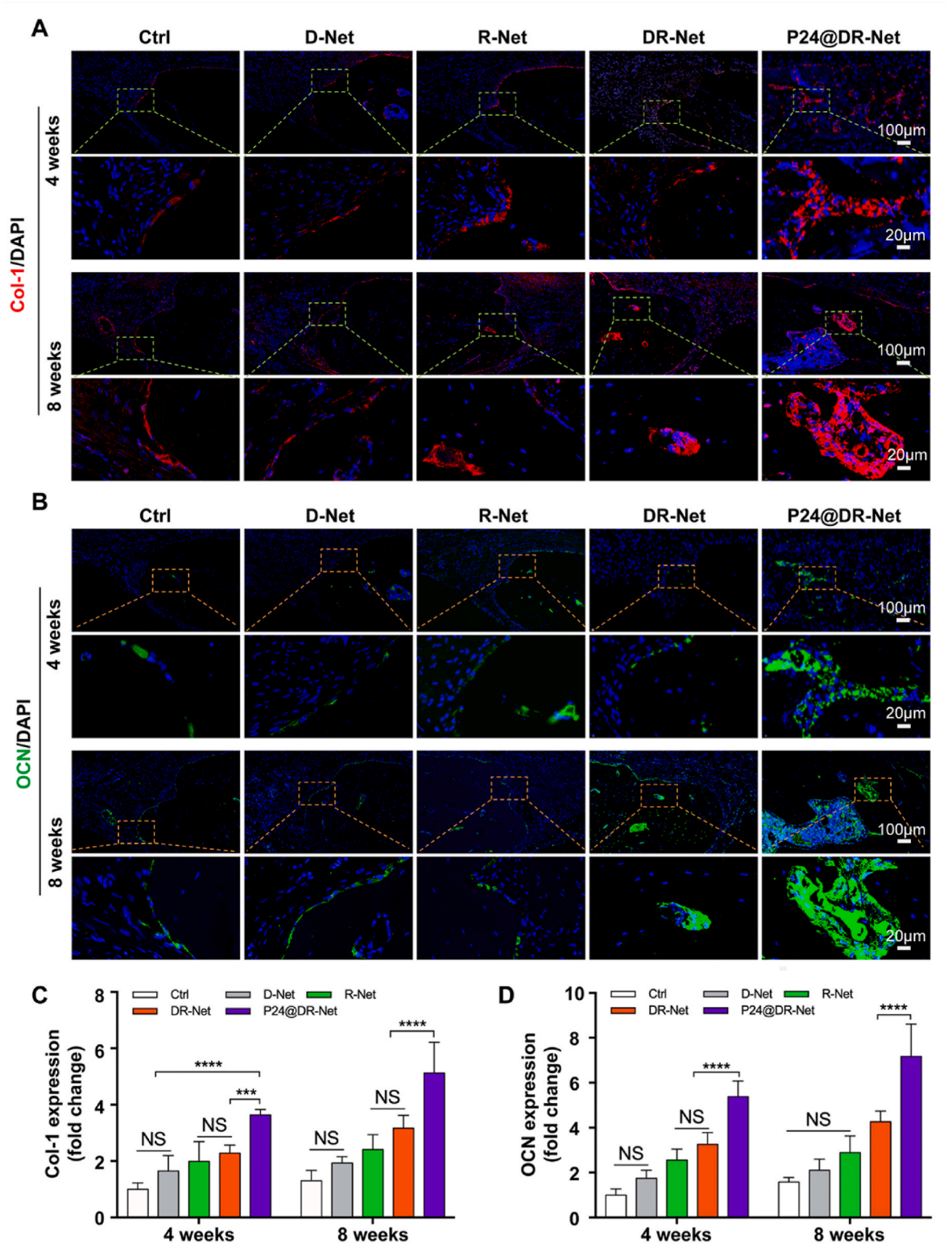

Fig. 7. Immunofluorescence analysis of the new formed tissue *in vivo*. Fluorescence images of A) Col-1 and B) OCN in each group respectively. Semi-quantitative analysis of C) Col-1 and D) OCN. (***p < 0.001 and ****p < 0.0001. "NS", no statistical significance. Data are presented as mean ± SD, n = 6. One-way ANOVA followed by Tukey's post hoc analysis was used).

groups with rigid covalent networks, such as R-Net, DR-Net, and P24@DR-Net, demonstrated comparatively enhanced levels of osteogenesis. This finding suggested that the D-Net hydrogel with a single dynamic network suffered from rapid degradation, prematurely losing its role as an osteoconductive scaffold. It is noteworthy that at 8 weeks, the BV/TV was significantly greater in the double-network group (DR-Net) than in the single-network groups (D-Net and R-Net) (Fig. 5E). This result revealed that double networks could further increase both the density and strength of the hydrogel with slow degradation rate, which can be effectively synchronized with bone formation, thereby

facilitating osteoconductivity. In addition, the sustained mechanical support provided by the double networks could also contribute to the osteogenic differentiation of stem cells to a certain extent. In conclusion, the double-network structure designed in this study can better fulfil the scaffold function and promote new bone formation.

To further enhance the osteoinductivity of the hydrogel scaffold, we introduced the active peptide P24 into the double-network structure. As expected, among all the groups, the P24@DR-Net hydrogel group demonstrated the highest degree of osteogenesis in the defective region, with well-integrated bone and strong growth of new bone from the edge to the center (Fig. 5D). Especially at 8 weeks, the P24@DR-Net treatment group exhibited almost complete filling of the bone defect area with newly formed bone tissue, indicating its most significant bone repair effect. As shown in Fig. 5E–H, the P24@DR-Net group demonstrated obviously increased BV/TV, Tb.N, and Tb.Th, with decreased Tb.Sp, compared to the other groups at 4 and 8 weeks. In addition, the P24@DR-Net group achieved more than 30 % BV/TV within 4 weeks, compared to only 22 % at 6 weeks for the previously reported commercial fibrin glue (FG) [58]. Hence, we speculate that the P24@DR-Net hydrogel can not only serve as a double-network scaffold with excellent osteoconductivity, but also exert osteoinductive effects through sustained release of the P24 peptide, thereby accelerating bone defect repair.

3.5. The histological evaluation in vivo

To further assess the *in vivo* osteogenesis-promoting effects of the P24@DR-Net hydrogel, this study employed H&E staining and Masson staining to evaluate bone regeneration in the defect area. The newly formed bone is denoted as NB, HB represents the host bone, and F indicates the fibrous tissue, with the area of the bone defect within the dashed box. H&E staining results were shown in Fig. 6A and **C**. Only limited new bone tissue appeared at the edges of the defective area, and the central part was composed of fibrous tissue in the control group. These findings suggest that bone defects cannot be self-healing in a 5 mm critical-sized calvarial defect model.

Moreover, there was no significant difference between the D-Net and the control groups (Fig. 6E, **F**). However, introducing the rigid network in DR-Net resulted in a comparatively more substantial degree of new bone formation within the defect area. These findings indicated that the pure dynamic network hydrogel (D-Net) degraded rapidly. On the other hand, the double-network hydrogel (DR-Net) reduced the degradation rate with enhanced bone guidance and mechanical support, providing a better match with the bone repair process. Over time, there was a progressive bone formation in all experimental groups. Notably, the P24@DR-Net hydrogel group exhibited abundant new bone formation around the periphery and a discernible trend of bone growth in the central area. At 8 weeks after surgery, the defect area was almost filled with newly generated bone tissue in the P24@DR-Net group. The results of Masson staining further corroborated those obtained from H&E staining (Fig. 6B, **D**).

Additionally, to investigate the effect of the P24@DR-Net hydrogel on collagen secretion by osteoblasts and mineralization of the bone matrix, immunofluorescence analysis was conducted at 4 and 8 weeks to examine the expression levels of the osteogenic markers (Col-1 and OCN proteins). Fig. 7A and **B** displayed the staining outcomes of Col-1 and OCN proteins in each group at 4 and 8 weeks. Over time, the expression of Col-1 and OCN showed an increasing trend based on quantitative analysis. (Fig. 7C, **D**). Consistent with the previous results, Col-1 and OCN expression levels were significantly higher in the P24@DR-Net group compared to the other groups. At 8 weeks, compared to the control group, the expression of Col-1 and OCN in the P24@DR-Net group showed a significant increase of 3.9 and 4.5 times, respectively. These findings suggested that the P24@DR-Net hydrogel could significantly promote osteoblasts to secrete bone matrix and mineralization. In summary, this kneadable dough-type hydrogel, P24@DR-Net, not only conforms to various irregular bone defects, but also rapidly promotes bone formation, demonstrating significant clinical application prospects.

4. Conclusion

In this study, we innovatively fabricated a dough-type hydrogel to repair irregular bone defects. The first dynamic network is constructed through S–Ag coordination bonds of 4-arm-PEG-SH and silver ions. It can match various irregular bone defects through kneading. Compared with D-Net, R-Net and the commercial fibrin glue, DR-Net demonstrate user-friendly operability during the process of filling uncontained alveolar bone defects. Furthermore, a second rigid covalent network was formed through photocrosslinking reaction of GelMA. The modulus of DR-Net increased by 8.6 times after irradiation and was 29 times that of the commercial fibrin glue. Therefore, the double-network hydrogel can effectively resist the external forces from surrounding tissues and maintain the space for bone regeneration. Furthermore, the P24 peptide with osteogenic activity was introduced to DR-Net through S–Ag coordination, which significantly promoted the sustained release process of P24 peptide, with 70 % released in 28 days, effectively accelerating the repair of critical cranial defects in rats. Overall, this dough-type hydrogel with kneadability, space-maintaining capacity, and osteogenic activity opens a new era for the treatment of irregular bone defects.

Ethics approval and consent to participate

In this study, all animal procedures were approved by the Animal Research Committee of Shanghai Jiao Tong University School of Medicine (SYXK 2018–0027).

CRediT authorship contribution statement

Ningtao Wang: Writing – original draft, Investigation, Formal analysis, Data curation, Conceptualization. **Jie Chen:** Writing – original draft, Data curation, Conceptualization. **Yanyang Chen:** Software, Methodology, Data curation. **Liang Chen:** Investigation, Data curation. **Luhan Bao:** Resources, Methodology. **Zhengmei Huang:** Methodology. **Xiaoyu Han:** Software. **Jiangkuo Lu:** Methodology. **Zhengwei Cai:** Writing – original draft, Funding acquisition, Formal analysis, Conceptualization. **Wenguo Cui:** Writing – review & editing, Supervision, Investigation, Funding acquisition, Conceptualization. **Zhengwei Huang:** Writing – review & editing, Supervision, Project administration, Funding acquisition, Data curation.

Declaration of competing interest

The authors declare no conflict of interest.

Acknowledgments

This work was supported by the National Natural Science Foundation of China (82071104/32101104/82202663), Science and Technology Commission of Shanghai Municipality (23XD1434200/22Y21901000), Program of Shanghai Academic/Technology Research Leader (22XD1422600), Shanghai Municipal Health Planning Commission (202140127), Shanghai Hospital Development Center (SHDC12022120).

Appendix A. Supplementary data

Supplementary data to this article can be found online at https://doi.org/10.1016/j.bioactmat.2024.06.021.

References

[1] Z. Zou, L. Wang, Z. Zhou, Q. Sun, D. Liu, Y. Chen, H. Hu, Y. Cai, S. Lin, Z. Yu, B. Tan, W. Guo, Z. Ling, X. Zou, Simultaneous incorporation of PTH (1-34) and nano-hydroxyapatite into Chitosan/Alginate Hydrogels for efficient bone regeneration, Bioact. Mater. 6 (6) (2020) 1839–1851, https://doi.org/10.1016/j.bioactmat.2020.11.021.

[2] Y. Liu, Z. Zhu, X. Pei, X. Zhang, X. Cheng, S. Hu, X. Gao, J. Wang, J. Chen, Q. Wan, ZIF-8-Modified multifunctional bone-adhesive hydrogels promoting angiogenesis and osteogenesis for bone regeneration, ACS Appl. Mater. Interfaces 12 (33) (2020) 36978–36995. https://pubs.acs.org/doi/10.1021/acsami.0c12090.

[3] D.F. Kinane, P.G. Stathopoulou, P.N. Papapanou, Authors' reply: predictive diagnostic tests in periodontal diseases, Nat. Rev. Dis. Prim. 3 (2017) 17070, https://doi.org/10.1038/nrdp.2017.70.

[4] D.O. Visscher, E. Farré-Guasch, M.N. Helder, S. Gibbs, T. Forouzanfar, P.P. van Zuijlen, J. Wolff, Advances in bioprinting technologies for craniofacial reconstruction, Trends Biotechnol. 34 (9) (2016) 700–710, https://doi.org/10.1016/j.tibtech.2016.04.001.

[5] Z. Hussain, S. Mehmood, X. Liu, Y. Liu, G. Wang, R. Pei, Decoding bone-inspired and cell-instructive cues of scaffolds for bone tissue engineering, Eng Regen 5 (1) (2024) 21–44, https://doi.org/10.1016/j.engreg.2023.10.003.

[6] Q. Li, W. He, W. Li, S. Luo, M. Zhou, D. Wu, Y. Li, S. Wu, Band-aid-like self-fixed barrier membranes enable superior bone augmentation, Adv. Sci. 10 (16) (2023) e2206981, https://doi.org/10.1002/advs.202206981.

[7] A. Scarano, F. Inchingolo, G. Murmura, T. Traini, A. Piattelli, F. Lorusso, Three-dimensional architecture and mechanical properties of bovine bone mixed with autologous platelet liquid, Blood, or physiological water: an in vitro study, Int. J. Mol. Sci. 19 (4) (2018) 1230, https://doi.org/10.3390/ijms19041230.

[8] F. Wang, D. Xia, S. Wang, R. Gu, F. Yang, X. Zhao, X. Liu, Y. Zhu, H. Liu, Y. Xu, Y. Liu, Y. Zhou, Photocrosslinkable Col/PCL/Mg composite membrane providing spatiotemporal maintenance and positive osteogenetic effects during guided bone regeneration, Bioact. Mater. 13 (2021) 53–63, https://doi.org/10.1016/j.bioactmat.2021.10.019.

[9] I. Lodoso-Torrecilla, J.J.J.P. van den Beucken, J.A. Jansen, Calcium phosphate cements: optimization toward biodegradability, Acta Biomater. 119 (2021) 1–12, https://doi.org/10.1016/j.actbio.2020.10.013.

[10] B. Magnan, M. Bondi, T. Maluta, E. Samaila, L. Schirru, C. Dall'Oca, Acrylic bone cement: current concept review, Musculoskelet Surg 97 (2) (2013) 93–100, https://doi.org/10.1007/s12306-013-0293-9.

[11] A. Sas, B. Helgason, S.J. Ferguson, G.H. van Lenthe, Mechanical and morphological characterization of PMMA/bone composites in human femoral heads, J. Mech. Behav. Biomed. Mater. 115 (2021) 104247, https://doi.org/10.1016/j.jmbbm.2020.104247.

[12] Ö. Demir-Oğuz, A.R. Boccaccini, D. Loca, Injectable bone cements: what benefits the combination of calcium phosphates and bioactive glasses could bring? Bioact. Mater. 19 (2023) 217–236, https://doi.org/10.1016/j.bioactmat.2022.04.007.

[13] A. Kirillova, C. Kelly, N. von Windheim, K. Gall, Bioinspired mineral-organic bioresorbable bone adhesive, Adv. Healthcare Mater. 7 (17) (2018) e1800467, https://doi.org/10.1002/adhm.201800467.

[14] A. Hoess, A. López, H. Engqvist, M. Karlsson Ott, C. Persson, Comparison of a quasi-dynamic and a static extraction method for the cytotoxic evaluation of acrylic bone cements, Mater. Sci. Eng., C 62 (2016) 274–282, https://doi.org/10.1016/j.msec.2016.01.048.

[15] Y. Ding, X. Liu, J. Zhang, Z. Lv, X. Meng, Z. Yuan, T. Long, Y. Wang, 3D printing polylactic acid polymer-bioactive glass loaded with bone cement for bone defect in weight-bearing area, Front. Bioeng. Biotechnol. 10 (2022) 947521, https://doi.org/10.3389/fbioe.2022.947521.

[16] Y.J. Wang, S.P. Shen, T.T. Hu, G.R. Williams, Y.Y. Bian, B. Feng, R.Z. Liang, X. S. Weng, Layered double hydroxide modified bone cement promoting osseointegration via multiple osteogenic signal pathways, ACS Nano 15 (6) (2021) 9732–9745, https://doi.org/10.1021/acsnano.1c00461.

[17] V.C. Panagiotopoulou, E. Santolini, E. Jones, A. Jha, P.V. Giannoudis, Adhesives for treatment of bone fractures: a review of the state-of-the art, Injury 53 (Suppl 2) (2022) S20–S25, https://doi.org/10.1016/j.injury.2021.02.019.

[18] L. Ding, H. Wang, J. Li, D. Liu, J. Bai, Z. Yuan, J. Yang, L. Bian, X. Zhao, B. Li, S. Chen, Preparation and characterizations of an injectable and biodegradable high-strength iron-bearing brushite cement for bone repair and vertebral augmentation applications, Biomater. Sci. 11 (1) (2023) 96–107, https://doi.org/10.1039/d2bm01535h.

[19] T. Lu, J. Wang, X. Yuan, C. Tang, X. Wang, F. He, J. Ye, Zinc-doped calcium silicate additive accelerates early angiogenesis and bone regeneration of calcium phosphate cement by double bioactive ions stimulation and immunoregulation, Biomater. Adv. 141 (2022) 213120, https://doi.org/10.1016/j.bioadv.2022.213120.

[20] W. Li, Y. Zheng, W. Pang, P. Lai, Bio-inspired adhesive hydrogel for wound healing, Biomed. Tech. 1 (2023) 65–72, https://doi.org/10.1016/j.bmt.2022.11.009.

[21] C. Liu, K. Peng, Y. Wu, F. Fu, Functional adhesive hydrogels for biological interfaces, Smart Med 2 (4) (2023) e20230024, https://doi.org/10.1002/SMMD.20230024.

[22] Z. Zhao, H. Ruan, A. Chen, W. Xiong, M. Zhang, M. Cai, W. Cui, Genetic engineered ultrasound-triggered injectable hydrogels for promoting bone reconstruction, Research 6 (2023) 221, https://doi.org/10.34133/research.0221.

[23] Z. Li, Y. Zhou, T. Li, J. Zhang, H. Tian, Stimuli-responsive hydrogels: fabrication and biomedical applications, View 3 (2) (2021) 20200112, https://doi.org/10.1002/VIW.20200112.

[24] H. Chopra, S. Kumar, I. Singh, Biopolymer-based scaffolds for tissue engineering applications, Curr. Drug Targets 22 (3) (2021) 282–295, https://doi.org/10.2174/1389450121999201102140408.

[25] S. Van Vlierberghe, P. Dubruel, E. Schacht, Biopolymer-based hydrogels as scaffolds for tissue engineering applications: a review, Biomacromolecules 12 (5) (2011) 1387–1408, https://doi.org/10.1021/bm200083n.

[26] J.D. Kretlow, S. Young, L. Klouda, M. Wong, A.G. Mikos, Injectable biomaterials for regenerating complex craniofacial tissues, Adv. Mater. 21 (32–33) (2009) 3368–3393, https://doi.org/10.1002/adma.200802009.

[27] D. Seliktar, Designing cell-compatible hydrogels for biomedical applications, Science 336 (6085) (2012) 1124–1128, https://doi.org/10.1126/science.1214804.

[28] K. Ren, C. He, C. Xiao, G. Li, X. Chen, Injectable glycopolypeptide hydrogels as biomimetic scaffolds for cartilage tissue engineering, Biomaterials 51 (2015) 238–249, https://doi.org/10.1016/j.biomaterials.2015.02.026.

[29] Z. Bi, X. Shi, S. Liao, X. Li, C. Sun, J. Liu, Strategies of immobilizing BMP-2 with 3D-printed scaffolds to improve osteogenesis, Regen. Med. 18 (2023) 425–441, https://doi.org/10.2217/rme-2022-0222.

[30] L. Shi, F. Wang, W. Zhu, Z. Xu, S. Fuchs, J. Hilborn, L. Zhu, Q. Ma, Y. Wang, X. Weng, D.A. Ossipov, Self-healing silk fibroin-based hydrogel for bone regeneration: dynamic metal-ligand self-assembly approach, Adv. Funct. Mater. 27 (37) (2017) 1700591–1700604, https://doi.org/10.1002/adfm.201700591.

[31] S.C. Grindy, R. Learsch, D. Mozhdehi, J. Cheng, D.G. Barrett, Z. Guan, P. B. Messersmith, N. Holten-Andersen, Control of hierarchical polymer mechanics with bioinspired metal-coordination dynamics, Nat. Mater. 14 (12) (2015) 1210–1216, https://doi.org/10.1038/nmat4401.

[32] K. Yue, G.T. Santiago, M.M. Alvarez, A. Tamayol, N. Annabi, A. Khademhosseini, Synthesis, properties, and biomedical applications of gelatin methacryloyl (GelMA) hydrogels, Biomaterials 73 (2015) 254–271, https://doi.org/10.1016/j.biomaterials.2015.08.045.

[33] D.L. Alge, K.S. Anseth, Bioactive hydrogels: lighting the way, Nat. Mater. 12 (11) (2013) 950–952, https://doi.org/10.1038/nmat3794.

[34] K. Modaresifar, A. Hadjizadeh, H. Niknejad, Design and fabrication of GelMA/chitosan nanoparticles composite hydrogel for angiogenic growth factor delivery, Artif. Cells, Nanomed. Biotechnol. 46 (8) (2018) 1799–1808, https://doi.org/10.1080/21691401.2017.1392970.

[35] Z. Chen, Z. Cai, C. Zhu, X. Song, Y. Qin, M. Zhu, T. Zhang, W. Cui, H. Tang, H. Zheng, Injectable and self-healing hydrogel with anti-bacterial and anti-inflammatory properties for acute bacterial rhinosinusitis with Micro invasive treatment, Adv. Healthcare Mater. 9 (20) (2020) e2001032, https://doi.org/10.1002/adhm.202001032.

[36] T. Ito, Y. Yeo, C.B. Highley, E. Bellas, D.S. Kohane, Dextran-based in situ cross-linked injectable hydrogels to prevent peritoneal adhesions, Biomaterials 28 (23) (2007) 3418–3426, https://doi.org/10.1016/j.biomaterials.2007.04.017.

[37] J. Li, J. Ma, Q. Feng, E. Xie, Q. Meng, W. Shu, J. Wu, L. Bian, F. Han, B. Li, Building osteogenic microenvironments with a double-network composite hydrogel for bone repair, Research 6 (2023) 21, https://doi.org/10.34133/research.0021.

[38] D. Li, K. Chen, H. Tang, S. Hu, L. Xin, X. Jing, Q. He, S. Wang, J. Song, L. Mei, R. D. Cannon, P. Ji, H. Wang, T. Chen, A logic-based diagnostic and therapeutic hydrogel with multistimuli responsiveness to orchestrate diabetic bone regeneration, Adv. Mater. 34 (11) (2022) e2108430, https://doi.org/10.1002/adma.202108430.

[39] X. Bai, M. Gao, S. Syed, J. Zhuang, X. Xu, X.Q. Zhang, Bioactive hydrogels for bone regeneration, Bioact. Mater. 3 (4) (2018) 401–417, https://doi.org/10.1016/j.bioactmat.2018.05.006.

[40] A. Nauth, J. Lane, J.T. Watson, P. Giannoudis, Bone graft substitution and augmentation, J. Orthop. Trauma 29 (Suppl 12) (2015) S34–S38, https://doi.org/10.1097/BOT.0000000000000464.

[41] J. Zhang, D. Tong, H. Song, R. Ruan, Y. Sun, Y. Lin, J. Wang, L. Hou, J. Dai, J. Ding, H. Yang, Osteoimmunity-regulating biomimetically hierarchical scaffold for augmented bone regeneration, Adv. Mater. 34 (36) (2022) e2202044, https://doi.org/10.1002/adma.202202044.

[42] Y.J. Seol, Y.J. Park, S.C. Lee, K.H. Kim, J.Y. Lee, T.I. Kim, Y.M. Lee, Y. Ku, I. C. Rhyu, S.B. Han, C.P. Chung, J. Biomed. Mater. Res. 77 (3) (2006) 599–607, https://doi.org/10.1002/jbm.a.30639.

[43] J. Li, L. Jin, M. Wang, S. Zhu, S. Xu, Repair of rat cranial bone defect by using bone morphogenetic protein-2-related peptide combined with microspheres composed of polylactic acid/polyglycolic acid copolymer and chitosan, Biomed. Mater. 10 (4) (2015) 045004, https://doi.org/10.1088/1748-6041/10/4/045004.

[44] Y. Liu, Z. Zhu, X. Pei, X. Zhang, X. Cheng, S. Hu, X. Gao, J. Wang, J. Chen, Q. Wan, ZIF-8-Modified multifunctional bone-adhesive hydrogels promoting angiogenesis and osteogenesis for bone regeneration, ACS Appl. Mater. Interfaces 12 (33) (2020) 36978–36995, https://doi.org/10.1021/acsami.0c12090.

[45] M.C. Embree, M. Chen, S. Pylawka, D. Kong, G.M. Iwaoka, I. Kalajzic, H. Yao, C. Shi, D. Sun, T.J. Sheu, D.A. Koslovsky, A. Koch, J.J. Mao, Exploiting endogenous fibrocartilage stem cells to regenerate cartilage and repair joint injury, Nat. Commun. 7 (2016) 13073, https://doi.org/10.1038/ncomms13073.

[46] S. Yao, X. Lin, Y. Xu, Y. Chen, P. Qiu, C. Shao, B. Jin, Z. Mu, N.A.J.M. Sommerdijk, R. Tang, Osteoporotic bone recovery by a highly bone-inductive calcium phosphate polymer-induced liquid-precursor, Adv. Sci. 6 (19) (2019) 1900683, https://doi.org/10.1002/advs.201900683.

[47] S. Yang, Z. Chen, P. Zhuang, Y. Tang, Z. Chen, F. Wang, Z. Cai, J. Wei, W. Cui, Seamlessly adhesive bionic periosteum patches via filling microcracks for defective bone healing, Small Methods 7 (10) (2023) e2300370, https://doi.org/10.1002/smtd.202300370.

[48] A.K. Gaharwar, S.M. Mihaila, A. Swami, A. Patel, S. Sant, R.L. Reis, A.P. Marques, M.E. Gomes, A. Khademhosseini, Bioactive silicate nanoplatelets for osteogenic

differentiation of human mesenchymal stem cells, Adv. Mater. 25 (24) (2013) 3329–3336, https://doi.org/10.1002/adma.201300584.
[49] T. Osathanon, C.M. Giachelli, M.J. Somerman, Immobilization of alkaline phosphatase on microporous nanofibrous fibrin scaffolds for bone tissue engineering, Biomaterials 30 (27) (2009) 4513–4521, https://doi.org/10.1016/j.biomaterials.
[50] Y.Y. Jiang, Z.F. Zhou, Y.J. Zhu, F.F. Chen, B.Q. Lu, W.T. Cao, Y.G. Zhang, Z.D. Cai, F. Chen, Enzymatic reaction generates biomimic nanominerals with superior bioactivity, Small 14 (51) (2018) e1804321, https://doi.org/10.1002/smll.201804321.
[51] M. Bruderer, R.G. Richards, M. Alini, M.J. Stoddart, Role and regulation of RUNX2 in osteogenesis, Eur. Cell. Mater. 28 (2014) 269–286, https://doi.org/10.22203/ecm.v028a19.
[52] A.K. Nagel, L.E. Ball, O-GlcNAc modification of the runt-related transcription factor 2 (Runx2) links osteogenesis and nutrient metabolism in bone marrow mesenchymal stem cells, Mol. Cell. Proteomics 13 (12) (2014) 3381–3395, https://doi.org/10.1074/mcp.M114.040691.
[53] Y. Arai, B. Choi, B.J. Kim, S. Park, H. Park, J.J. Moon, S.H. Lee, Cryptic ligand on collagen matrix unveiled by MMP13 accelerates bone tissue regeneration via MMP13/Integrin α3/RUNX2 feedback loop, Acta Biomater. 125 (2021) 219–230, https://doi.org/10.1016/j.actbio.2021.02.042.
[54] Z. Zhou, Y. Fan, Y. Jiang, S. Shi, C. Xue, X. Zhao, S. Tan, X. Chen, C. Feng, Y. Zhu, J. Yan, Z. Zhou, Y. Zhao, J. Liu, F. Chen, S. He, Mineralized enzyme-based biomaterials with superior bioactivities for bone regeneration, ACS Appl. Mater. Interfaces 14 (32) (2022) 36315–36330, https://doi.org/10.1021/acsami.2c05794.
[55] X. Han, J. Shen, S. Chen, Z. Cai, Y. Zhu, W. Yi, K. Li, W. Cai, B. Tao, W. Cui, D. Bai, Ultrasonic-controlled "explosive" hydrogels to precisely regulate spatiotemporal osteoimmune disturbance, Biomaterials 295 (2023) 122057, https://doi.org/10.1016/j.biomaterials.2023.122057.
[56] Y. Yang, T. Xu, Q. Zhang, Y. Piao, H.P. Bei, X. Zhao, Biomimetic, stiff, and adhesive periosteum with osteogenic-angiogenic coupling effect for bone regeneration, Small 17 (14) (2021) e2006598, https://doi.org/10.1002/smll.202006598.
[57] H. Wei, B. Zhang, M. Lei, Z. Lu, J. Liu, B. Guo, Y. Yu, Visible-light-mediated nano-biomineralization of customizable tough hydrogels for biomimetic tissue engineering, ACS Nano 16 (3) (2022) 4734–4745, https://doi.org/10.1021/acsnano.1c11589.
[58] C.H. Reis, R.L. Buchaim, K.T. Pomini, A.L. Hamzé, I.V. Zattiti, M.A. Duarte, M. P. Alcalde, B. Barraviera, R.S. Ferreira Júnior, F.M. Pontes, C.R. Grandini, A. D. Ortiz, S.O. Fideles, R.M. Eugênio, G.M. Rosa Junior, D.D. Teixeira, E.D. Pereira, J.P. Pilon, M.A. Miglino, D.V. Buchaim, Effects of a biocomplex formed by two scaffold biomaterials, hydroxyapatite/tricalcium phosphate ceramic and fibrin biopolymer, with photobiomodulation, on bone repair, Polymers 14 (10) (2022) 2075, https://doi.org/10.3390/polym14102075.